Society of Medical Education & Research

2022, Volume 2, Issue 1, Page No: 155-176
ISSN: 3108-4826

Journal of Medical Sciences and Interdisciplinary Research

Loss of CXCL12 Drives Colorectal Cancer Progression and Impairs Anti-PD-L1 Immunotherapy via MDSC Modulation

Natalie Rose Bennett[1], Oliver James King[1]*, Julien Marc Lefevre[2], Antoine Pascal Durand[2]

[1]Department of Management, University of Sussex Business School, Brighton, United Kingdom.
[2]Department of Management, KEDGE Business School, Marseille, France.

***E-mail** ✉ n.bennett.sussex@yahoo.com

Abstract

Numerous approaches targeting the CXCL12 pathway, particularly CXCR4 inhibitors, have been explored for treating colorectal cancer (CRC). Although these methods have demonstrated partial success in clinical studies, the reasons why reduced CXCL12 levels impair the effectiveness of anti-PD-L1 therapy—a major obstacle in immunotherapy—remain poorly understood, underscoring the necessity for further mechanistic investigation and improved therapeutic approaches. This research combined single-cell transcriptomic sequencing, in vitro cellular assays, and in vivo animal models to detect CXCL12-associated RNA-binding proteins (RBPs) with causal connections to CRC, pinpoint critical cell populations involved in resistance, and confirm underlying mechanisms. Twelve RBPs linked to CXCL12 exhibited causal associations with CRC. Using machine learning techniques and diagnostic evaluations, CPEB3, DDX39B, and SIDT2 emerged as potential CRC biomarkers. Monocytes were identified as the primary cell type in CRC due to their expression patterns of these biomarkers. Single-cell transcription factor profiling revealed two key CRC-associated factors: MEIS2 and TCF4. Both in vitro and in vivo experiments demonstrated that silencing CXCL12 enhanced the migratory and invasive abilities of CRC cells. Significantly, combining CXCL12 overexpression with PD-L1 blockade resulted in the greatest reduction in cell viability and invasiveness, suggesting that CXCL12 potentiates rather than hinders anti-PD-L1 treatment efficacy. Additionally, CXCL12 levels showed a negative correlation with the abundance and quantity of myeloid-derived suppressor cells. The discovery of CPEB3, DDX39B, and SIDT2 as biomarkers tied to CXCL12 in CRC, along with evidence connecting CXCL12 to MDSC modulation and resistance to anti-PD-L1 therapy, offers a new perspective on immunotherapy failure in CRC. These insights could inform the design of clinical treatment protocols and support the creation of CXCL12-based combination therapies to surmount anti-PD-L1 resistance and enhance immunotherapy results in CRC.

Keywords: Colorectal cancer, CXCL12, RNA-binding protein genes, Anti-PD-L1 immunotherapy, Monocytes, Myeloid-derived suppressor cells

Introduction

Colorectal cancer (CRC) ranks among the most prevalent malignant neoplasms of the gastrointestinal system, with elevated global incidence and mortality rates [1]. Current management options encompass surgical excision, neoadjuvant and adjuvant chemoradiotherapy, molecular targeted agents, and immunotherapy, though surgery remains the cornerstone. Despite these interventions, CRC retains high recurrence risks and substantial 5-year post-surgical mortality [2, 3]. Thus, a deeper understanding of the molecular events driving CRC onset and progression is essential to improve prognostic tools. CRC development is marked by specific genetic and epigenetic alterations [4]. Recent data highlight a substantial impact of RNA-binding proteins (RBPs), which primarily regulate RNA processing and trafficking, on CRC advancement [4-6]. For instance, RBPs influence patient outcomes in CRC [7], facilitate cellular proliferation and tumorigenesis [8], and can act as suppressors by altering JAK/STAT pathways [9].

Access this article online https://smerpub.com/

Received: 11 March 2022; **Accepted:** 02 June 2022

How to cite this article: Bennett NR, King OJ, Lefevre JM, Antoine Pascal Durand AP. Loss of CXCL12 Drives Colorectal Cancer Progression and Impairs Anti-PD-L1 Immunotherapy via MDSC Modulation. J Med Sci Interdiscip Res. 2022;2(1):15-76.https://doi.org/10.51847/c2qR6ArN0J

Collectively, these observations underscore the significance of RBPs in CRC and suggest that RBP-related genes may function as diagnostic markers while contributing to cancer cell motility and spread.

Metastasis driven by tumor cell migration accounts for most deaths in colon cancer [10, 11]. The chemokine CXCL12 plays a central role in promoting CRC invasion and migration. Prior investigations into CXCL12-driven CRC progression and treatment resistance have largely concentrated on classical downstream signaling routes, including PI3K/AKT/mTOR, MEK/ERK, and Wnt/β-catenin cascades, emphasizing transcriptional control. Although valuable, this focus has neglected RBP-governed RNA metabolic regulation, which may critically influence anti-PD-L1 resistance through post-transcriptional modulation of pivotal effectors [12]. CXCL12 is highly expressed in frequent CRC metastatic sites such as lymph nodes and liver, while its receptor CXCR4 is overexpressed in CRC tissues [13]. The CXCR4/CXCL12 axis appears to facilitate CRC metastasis; ligand binding activates diverse pathways that boost tumor proliferation, migration, and invasion [14, 15]. These include PI3K/AKT/mTOR, MEK/ERK, and Wnt/β-catenin signaling, which support cell survival, angiogenesis, and immune evasion, thereby fueling tumor expansion and dissemination [16-18].

Various countermeasures targeting CXCL12 have been developed, such as CXCR4 blockers, pathway-specific inhibitors, immunotherapeutic agents, and genetic approaches. Some clinical promise has been observed, yet additional refinement is required. Considering the limited exploration of post-transcriptional control in CXCL12 signaling alongside the documented involvement of RBPs in CRC, examining CXCL12-linked RBPs provides a fresh avenue to elucidate novel contributors to anti-PD-L1 resistance beyond conventional cytokine pathways. Accordingly, this study employed single-cell transcriptomic analysis to assess the involvement of CXCL12-associated RBP genes in CRC progression, with particular attention to their potential influence on PD-L1 levels and myeloid-derived suppressor cell (MDSC) recruitment in CRC.

Materials and Methods

Data acquisition

Datasets from TCGA and GTEx covering 33 cancer types were downloaded via the UCSC Xena browser. In addition, RNA-seq data and corresponding clinical details (including survival outcomes) for colorectal cancer (CRC) cases were obtained from Xena and GEO repositories. The datasets GSE14297, GSE21510, GSE23878, GSE81558, GSE89076, and GSE90627 were employed to assess CXCL12 levels. The TCGA-CRC cohort, comprising 469 CRC cases and 349 healthy controls (HC), served as the primary training set [19]. Validation of the prognostic risk score utilized the GSE39582 (including 566 CRC cases with survival data and 19 HC) and GSE87211 (including 203 CRC cases with survival data and 160 HC) datasets [20]. For single-cell analyses, the GSE146771 cohort with 10 CRC and 10 HC specimens was applied [21]. CRC genetic variants (GCST90428118) were sourced from the GWAS Catalog, encompassing 4988 CRC cases and 310272 controls [22]. Cis-eQTL data for relevant exposures were retrieved from the eQTLGen Consortium [23]. Furthermore, a collection of 1,542 RNA-binding protein-related genes (RBP-RGs) was compiled from prior research [24].

Analysis of CXCL12 expression and prognostic significance

CXCL12 levels were initially compared between neoplastic and adjacent non-tumor tissues across 33 cancer types. Subsequent evaluation focused on CXCL12 in CRC-specific cohorts (GSE14297, GSE21510, GSE23878, GSE81558, GSE89076, and GSE90627). Kaplan-Meier overall survival (OS) plots were generated to evaluate CXCL12's prognostic relevance using the "survminer" R package (version 0.4.9).

Identification of potential CRC biomarkers

Differential expression analysis was conducted on 469 CRC versus 349 HC specimens from the TCGA-CRC cohort, with criteria of $|\log2FC| > 1$ and adjusted p-value < 0.05 via the "DESeq2" R package (version 1.48) [25]. Genes correlated with CXCL12 were identified using Spearman correlation ($|Cor| > 0.6$, $p < 0.05$). Overlapping genes among differentially expressed genes (DEGs), the 1,542 RBP-RGs, and CXCL12-correlated genes were determined with the "venn" package (version 1.11).

Genes exhibiting causal links to CRC were selected through Mendelian randomization (MR). SNPs passing FDR < 0.05 and MAF > 0.01 were preprocessed in SMR software (version 1.03), excluding linked variants ($r^2 = 0.1$, window = 500 kb, F-statistic < 10). Two-sample MR was performed with the "TwoSampleMR" package (version 0.5.6), confirming causal effects of exposures (candidate genes) on outcomes via Steiger filtering.

From causally related candidates, feature importance was ranked using three algorithms (LASSO regression, SVM-RFE, and random forest). Final target genes emerged from the intersection of top features across these methods.

Receiver operating characteristic (ROC) curves for target genes were plotted in TCGA-CRC, GSE39582, and GSE87211 cohorts to detect CRC biomarkers (AUC > 0.7). A nomogram and associated calibration plot were developed for CRC risk assessment using the "RMS" package (version 6.5–0).

Development of a prognostic risk score for CRC

The risk score was derived as Riskscore = ∑βiXi. Risk distribution plots, Kaplan-Meier OS curves, and ROC analyses assessed model performance. External cohorts GSE39582 and GSE87211 provided independent validation.

Cell type characterization and identification of critical CRC subpopulations

The GSE146771 cohort includes immune-enriched specimens from CRC tumors and matched normal tissues, offering a valuable model for examining immune composition and CXCL12-driven interactions, distinct from tumor-intrinsic effects. To elucidate single-cell mechanisms of CXCL12-linked resistance to anti-PD-L1 therapy after pan-cancer and RBP analyses, scRNA-seq from GSE146771 was used to profile CXCL12 and related regulators at cellular resolution.

Quality filtering of GSE146771 was executed in "Seurat" (version 4.0.0). Cells exceeding 20% mitochondrial content, with <200 or >6000 detected genes, were removed to eliminate poor-quality or doublet cells. Normalization applied "LogNormalize" (scale factor = 10,000), and highly variable features were selected via "FindVariableFeatures" (method = "vst", nfeatures = 2000) [26].

Cell clustering and visualization

Following data scaling and principal component analysis (PCA, npcs = 50), cells were grouped into clusters via the "FindNeighbors" and "FindClusters" functions (resolution = 0.5). Dimensionality reduction for visualization was achieved with UMAP through the "RunUMAP" function, utilizing the top 50 principal components (npcs = 50) and a minimum distance parameter of 0.3 to enhance cluster distinction. Annotation of cell types relied on markers from the CellMarker database, applying a correlation threshold of at least 0.7 for confident assignment. Differences in cell type proportions between CRC and HC samples were assessed statistically with the Wilcoxon rank-sum test. Pathway enrichment and functional analysis of differentially represented cells were conducted using ReactomeGSA.

Visualization of CXCL12 and biomarker distribution across cell types

UMAP projections were generated to display the localization of CXCL12 and identified biomarkers within various cell populations. Cells exhibiting statistically significant differences in CXCL12 levels were designated as critical subpopulations. These key cells underwent further subclustering with "FindNeighbors" and "FindClusters" (resolution = 1), followed by UMAP visualization. Pseudotime trajectory analysis for differentiation within key cells was performed using Monocle2, and dynamic gene expression along the trajectory was evaluated via the "differentialGeneTest" function. Intercellular communication was inferred to assess receptor-ligand pairing involving key cells, utilizing the "CellChat" package with the CellChatDB database. P-value adjustment employed the Benjamini-Hochberg procedure, with significance defined as FDR < 0.05.

Single-Cell transcription factor analysis

A random forest model was built using the single-cell expression matrix, with transcription factors (TFs) as features and CXCL12 expression as the target variable. Importance metrics for each TF relative to CXCL12 were derived to define co-expression modules. Motif enrichment for genes within each module was performed against a gene-motif database using "RcisTarget." Predicted target genes for significantly enriched motifs were identified, enabling the construction of regulatory networks (regulons) comprising TFs and their targets. Regulon activity scores across cells were computed with "AUCell."

In vitro validation of CXCL12 expression and regulation

Normal human colonic epithelial cells (FHC) and colorectal cancer cells (HT-29) were employed to confirm CXCL12 and biomarker expression levels. Gene and protein expression of CXCL12 and associated biomarkers in FHC and HT-29 lines were quantified by qRT-PCR and Western Blot, respectively. Cell models

with CXCL12 knockdown or overexpression were established (FHC-NC, FHC-siCXCL12, FHC-oeCXCL12, HT-29-NC, HT-29-siCXCL12, and HT-29-oeCXCL12), and biomarker levels were measured using qRT-PCR and Western Blot. Primers targeted coding sequences of genes of interest, with GAPDH serving as the housekeeping control. Primer details are provided in **Table 1.**

Table 1. Primer sequences

Gene Target	Primer Orientation	Nucleotide Sequence (5′–3′)
CXCL12	Forward primer	GAGAGCCAACGTCAAGCATCTG
	Reverse primer	TCCTTTAGCTTCGGGTCAATGC
CPEB3	Forward primer	ATGGCAGACAAGGTGAAGCTGA
	Reverse primer	TCCTTGGTGCTGATGTTGCTGT
DDX39B	Forward primer	GGAGAACATCGAGTGGCTGAAG
	Reverse primer	CCAGTCTTGGTGATGCTGTTGA
SIDT2	Forward primer	AGACGGCTACCTGAACGAGTTC
	Reverse primer	TGGTGATGCTGTTGAAGGTGAC
GAPDH	Forward primer	GAAGGTGAAGGTCGGAGTCAA
	Reverse primer	GAAGATGGTGATGGGATTTC

To investigate CXCL12 transcriptional control, HT-29 models with silenced or overexpressed TFs were generated, and subsequent CXCL12 mRNA and protein levels were assessed. Intracellular co-localization between CXCL12 and candidate upstream TFs, along with direct transcriptional effects, was examined via a dual-luciferase allele-specific expression reporter assay.

In vitro functional assessment of CXCL12

The impact of CXCL12 knockdown or overexpression on CRC cell proliferation, migration, and invasion was evaluated through CCK-8 proliferation assays, EdU incorporation staining, colony formation assays, and Transwell migration/invasion experiments.

In vivo validation of CXCL12 expression and function

Female BALB/c nude mice (aged 6–8 weeks, immunodeficient) were utilized for in vivo studies of CXCL12 and biomarker expression. Animals were allocated randomly to a negative control group (n = 8, WT), a positive control tumor-bearing group (n = 48, Model), and a treatment group (n = 48, siCXCL12-Model). Experimental mice received subcutaneous injections of CXCL12-silenced HT-29 cells (1 × 10^7 cells/mouse), positive controls were injected with unmodified HT-29 cells (1 × 10^7 cells/mouse), and negative controls received equivalent volumes of saline. Weekly monitoring included body weight recording. Tumor dimensions were measured weekly with calipers, and volume was estimated as (length × width²)/2. At 6 weeks, mice were euthanized, with the collection of serum and colorectal tissues. Tissues and lymph nodes underwent hematoxylin-eosin (HE) staining for histopathological evaluation. Ki-67 immunohistochemistry was performed on tumor sections to quantify proliferation in response to altered CXCL12 levels. Tumor samples were dissociated into single-cell suspensions via mechanical grinding and enzymatic digestion, followed by removal of debris and erythrocytes through centrifugation and rinsing to yield enriched tumor cell preparations. Expression of CXCL12 and biomarkers was analyzed in these cells. Additionally, the influence of CXCL12 modulation on the proliferation, migration, and invasion of tumor cells in vivo was examined using CCK-8, EdU, colony formation, and Transwell assays on isolated cells.

In vitro investigation of CXCL12-mediated primary resistance to anti-PD-L1 therapy

HT-29 cells exhibiting elevated CXCR4 levels were selected to examine how CXCL12 contributes to primary resistance against anti-PD-L1 treatment. Experimental conditions included: Con (no treatment), CXCL12si (CXCL12 knockdown), CXCL12oe (CXCL12 overexpression), Con + anti-PD-L1, and CXCL12oe + anti-PD-L1. Cell proliferation across groups was assessed via CCK-8 assays. Peripheral blood mononuclear cells were co-cultured with these treated HT-29 groups, and changes in the proportion and count of critical cell populations were evaluated by flow cytometry. Myeloid-derived suppressor cells (MDSCs) were characterized as follows: monocytic MDSCs (M-MDSCs) identified as CD14+ HLA-DRlow/- CD11b+ cells, and granulocytic MDSCs (G-MDSCs) as CD15+ CD11b+ HLA-DRlow/- cells. Subset proportions and cell numbers were quantified using FlowJo software.

Statistical methods

Results are reported as mean ± SD. Comparisons involving three or more groups employed one-way ANOVA with Tukey's post-hoc test when parametric assumptions held; otherwise, the Kruskal-Wallis test with Dunn's correction was applied. Multiple comparisons were adjusted via the Benjamini-Hochberg (BH) procedure. All in vitro assays included at least three biological replicates and three technical replicates per condition. Data normality was tested using Shapiro–Wilk, and variance homogeneity via Levene's test. ROC curves were generated, with AUC and 95% confidence intervals computed by the DeLong method. Prognostic models were assessed through the concordance index (C-index) with bootstrap adjustment and calibration plots. All tests were two-sided, with statistical significance set at $\alpha = 0.05$.

Results and Discussion

CXCL12 expression linked to colorectal cancer risk

CXCL12 displayed markedly elevated levels in four tumor types: DLBC, GBM, LAML, and TGCT. In contrast, significantly reduced expression was observed in 21 cancers: ACC, BLCA, BRCA, CESC, CHOL, COAD, ESCA, HNSC, KICH, KIRC, KIRP, LIHC, LUAD, LUSC, MESO, PAAD, PRAD, READ, SKCM, STAD, and UCEC ($p < 0.05$) **(Figure 1a).** Within CRC-specific cohorts, CXCL12 was consistently downregulated across GSE14297, GSE21510, GSE23878, GSE81558, GSE89076, and GSE90627 datasets ($p < 0.01$) **(Figures 1b–g).** Overall survival differed significantly between high- and low-expression groups in the TCGA-COAD cohort ($p = 0.0145$) **(Figures 1h–i).**

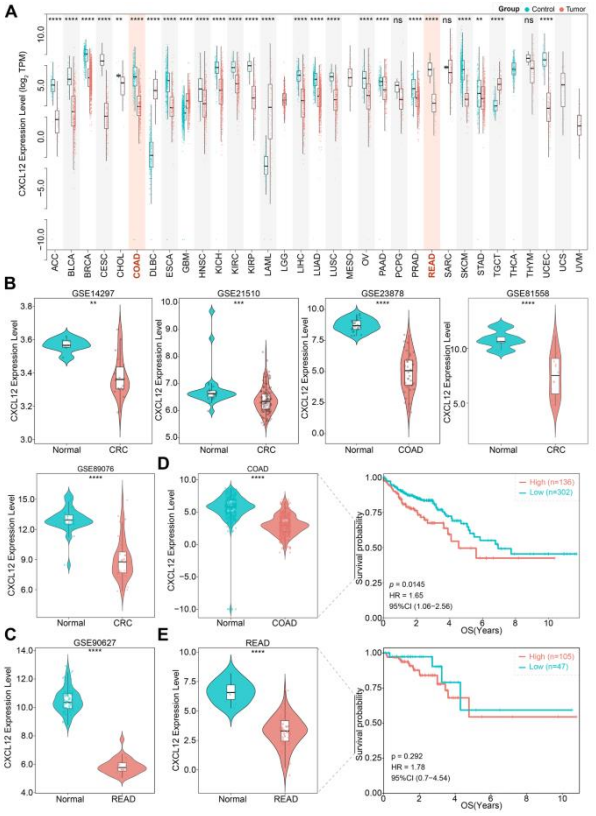

Figure 1. CXCL12 and its association with colorectal cancer (CRC) risk. (A) CXCL12 levels across 33 cancer types. (B) CXCL12 expression in colon adenocarcinoma (COAD) datasets (GSE14297, GSE21510, GSE23878, GSE81558, and GSE89076). (C) CXCL12 expression in rectal adenocarcinoma (READ) dataset (GSE90627). (D) Kaplan-Meier survival analysis for CXCL12 in TCGA-COAD. (E) Kaplan-Meier survival analysis for CXCL12 in TCGA-READ. indicates intergroup differences. COAD and READ represent histological subtypes of CRC; $p < 0.05$, $p < 0.01$, $p < 0.001$, $p < 0.0001$.

CPEB3, DDX39B, and SIDT2 identified as CRC Biomarkers

Differential expression analysis in the TCGA-CRC cohort (469 CRC vs. 349 HC samples) revealed 12,641 DEGs (6,087 upregulated, 6,554 downregulated). Correlation screening yielded 133 genes associated with CXCL12. Overlap among these 12,641 DEGs, 133 CXCL12-correlated genes, and 1,542 RBP-related genes produced 15 candidates: CPEB3, DDX39B, EIF4E3, MBNL1, MYEF2, NANOS1, RBM20, RBM24, RBM6, RBPMS2, SAMHD1, SIDT2, TDRD9, ZC3H12C, and ZGPAT. Among these, DDX39B, MBNL1, NANOS1,

SAMHD1, ZC3H12C, and ZGPAT exhibited significant upregulation in CRC tissues **(Figure 2a).**

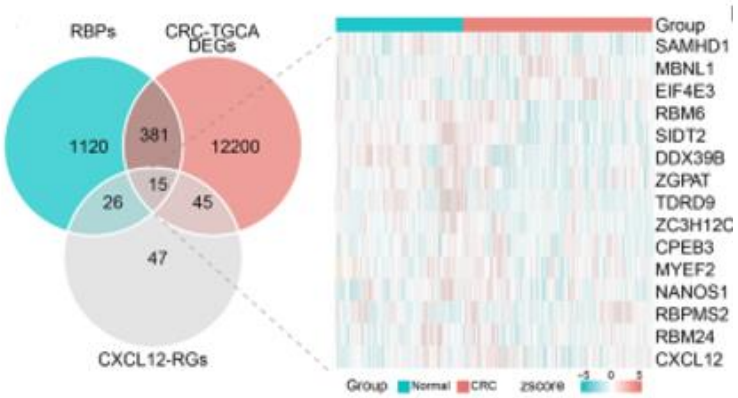

a)

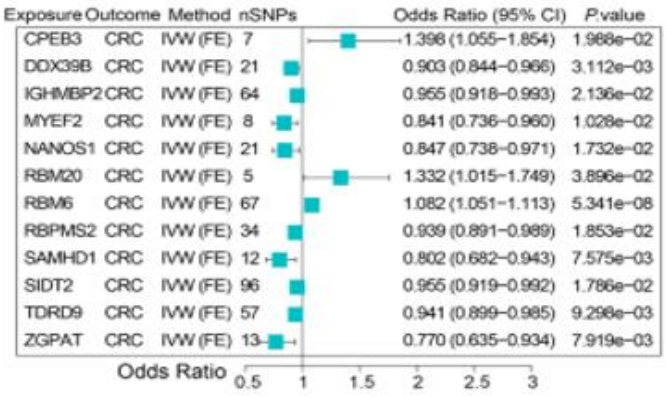

b)

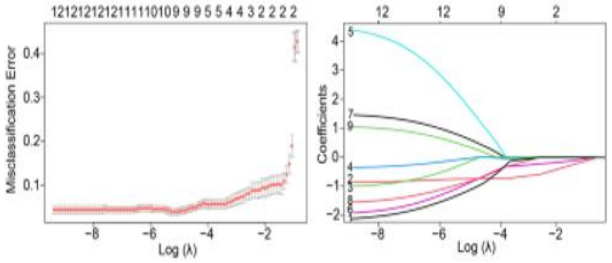

c)

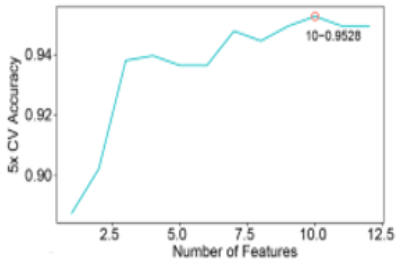

d)

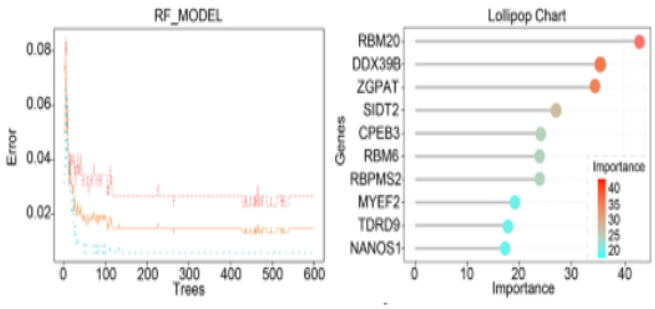

e)

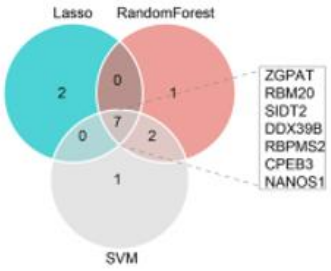

f)

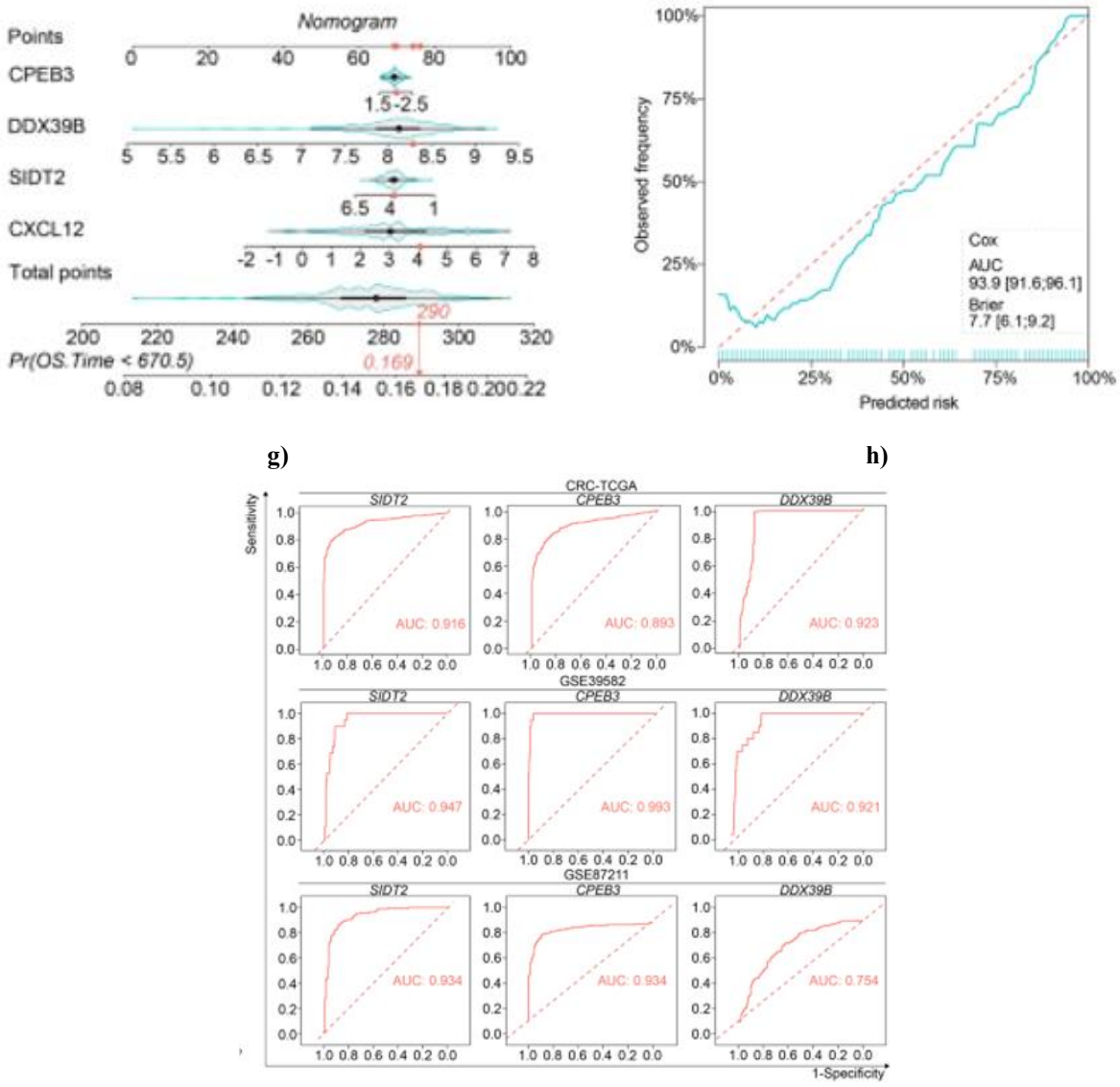

Figure 2. Discovery of colorectal cancer (CRC) biomarkers. (a) Venn diagram illustrating 15 overlapping candidate genes. (b) Genes with established causal links to CRC. (c–e) Feature selection via three machine learning approaches: (c) LASSO regression, (d) SVM-RFE, and (e) random forest. (f) Venn diagram of final target genes. (g) ROC curves for biomarkers across CRC cohorts (TCGA-CRC, GSE39582, and GSE87211). (h) Nomogram incorporating three biomarkers. (i) Calibration plot for the nomogram.

Mendelian randomization outcomes indicated that 12 genes exhibited causal associations with CRC: CPEB3, RBM20, and RBM6 linked to favorable CRC prognosis, while DDX39B, IGHMBP2, MYEF2, NANOS1, RBPMS2, SAMHD1, SIDT2, TDRD9, and ZGPAT correlated with adverse outcomes **(Figure 2b).** From these 12 candidates, LASSO identified 9 signature genes, SVM-RFE selected 10, and random forest yielded 10 **(Figures 2c–e).** Intersection across the three feature sets produced seven core targets: CPEB3, DDX39B, NANOS1, RBM20, RBPMS2, SIDT2, and ZGPAT **(Figure 2f).** Of these, CPEB3, DDX39B, and SIDT2 achieved AUC values exceeding 0.7 across all evaluated cohorts (TCGA-CRC, GSE39582, and GSE87211) **(Figure 2g).** Accordingly, CPEB3, DDX39B, and SIDT2 were designated as CRC biomarkers, and a predictive nomogram was developed incorporating these three. The nomogram demonstrated strong calibration, with

predicted risks aligning closely with observed probabilities, confirming its diagnostic accuracy **(Figures 2h–i).**

A prognostic risk model for CRC was established using CPEB3, DDX39B, and SIDT2, where CPEB3 acted as a protective factor, whereas DDX39B and SIDT2 served as risk-promoting factors. Marked survival disparities emerged between healthy control and high-risk CRC groups (p = 0.017). Three-year survival prediction yielded AUC values above 0.6 **(Figures 3a–c).** Validation in GSE39582 and GSE87211 cohorts showed risk distributions, Kaplan-Meier curves, and ROC performance consistent with the TCGA-CRC training set **(Figures 3d–f and 3g–i).**

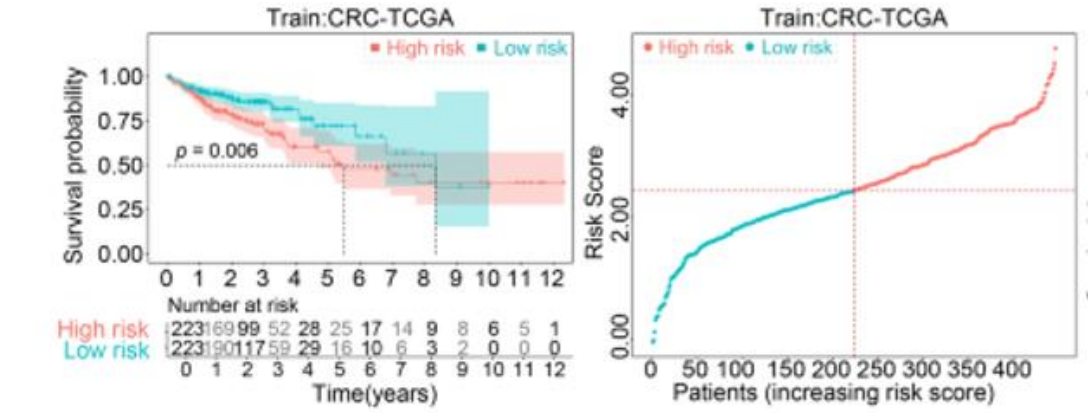

a)

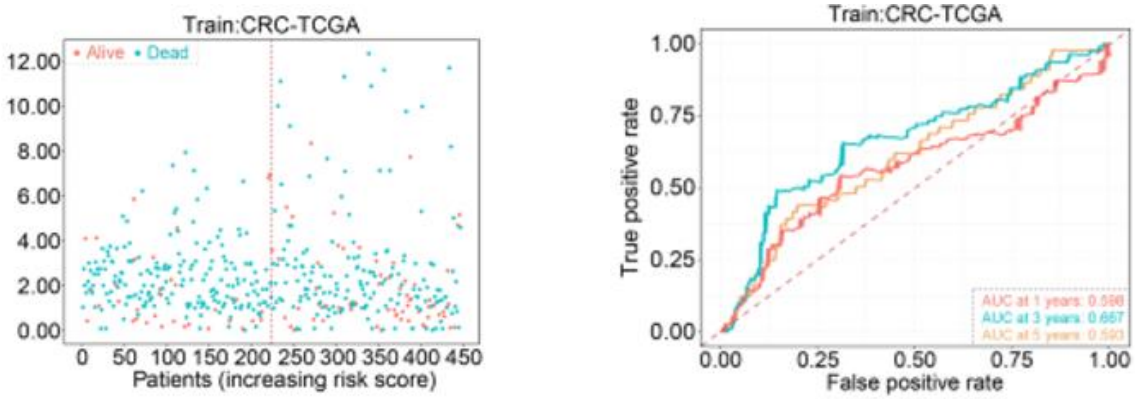

b) c)

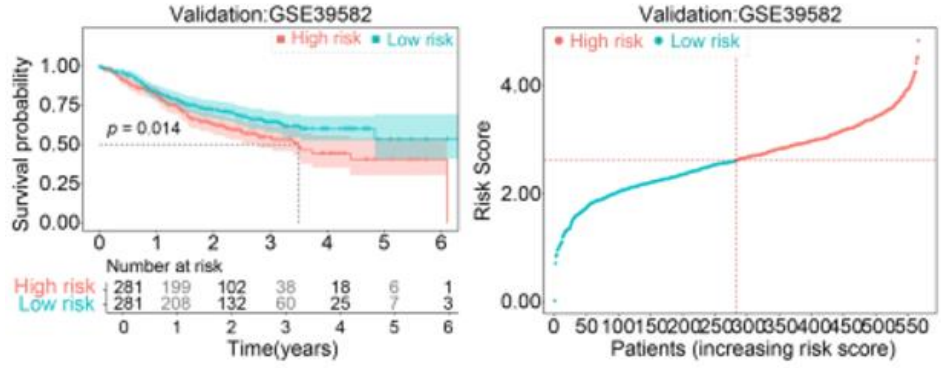

d)

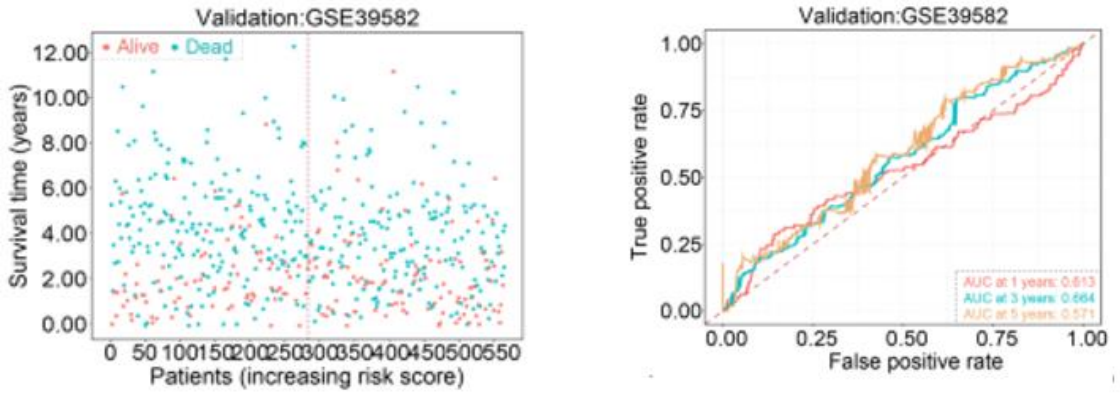

e) f)

Figure 3. Prognostic risk assessment for colorectal cancer (CRC). (A) Risk distribution plot for the model in TCGA-CRC (training cohort). (B) Kaplan-Meier survival analysis in TCGA-CRC. (C) ROC curve for the model in TCGA-CRC. (D) Risk distribution in GSE39582. (E) Kaplan-Meier curve in GSE39582. (F) ROC curve in GSE39582. (G) Risk distribution in GSE87211. (H) Kaplan-Meier curve in GSE87211. (I) ROC curve in GSE87211.

Monocytes emerged as the critical cell population in CRC

Quality filtering was applied to the GSE146771 dataset, followed by selection of the top 2,000 highly variable genes for downstream normalization **(Figures 4a–b).** Clustering resolved cells into 29 groups, annotated as 6 major types: CD8+ T cells, CD4+ T cells, B cells, monocytes, NK cells, and hematopoietic stem cells (HSC) **(Figure 4c).** All 6 populations were significantly enriched in CRC relative to controls ($p < 0.001$) **(Figures 4d–e).** CXCL12 displayed predominant expression restricted to monocytes, with marked differences between CRC and healthy samples, leading to the designation of monocytes as the primary CRC-associated cell type **(Figures 4f–g).**

Subclustering of monocytes along cell cycle phases revealed 7 distinct subtypes, with most signature markers peaking in later differentiation phases **(Figure 4h).** Intercellular signaling was notably reduced in CRC, positioning monocytes as the central hub for communication. The dominant ligand-receptor pair between HSC and CD8+ T cells was MIF-(CD74+CXCR4), while ANXA1–FPR1 predominated between HSC and monocytes in the CRC context **(Figure 4i).**

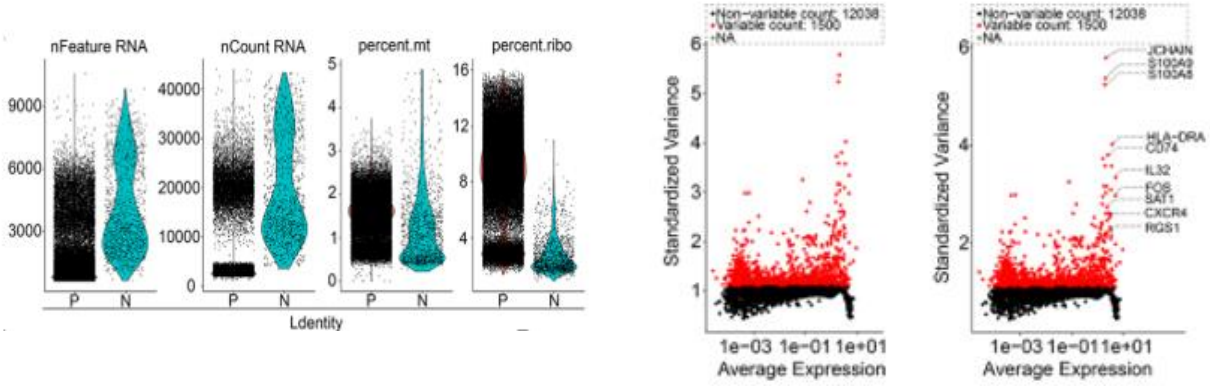

a) b)

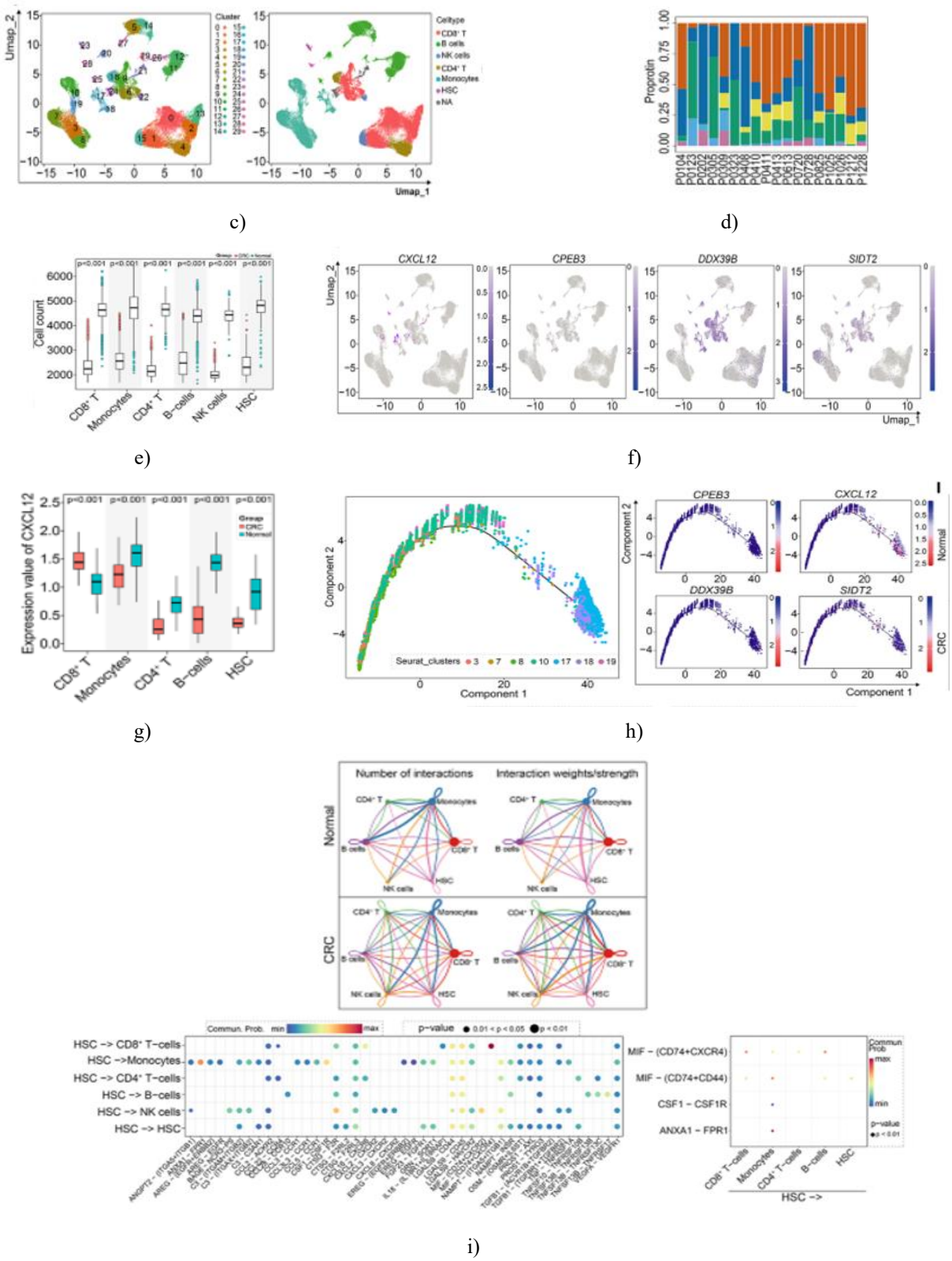

Figure 4. Single-cell profiling and intercellular interaction analysis. (a) Quality assessment of GSE146771. (b) Selection of the top 2,000 highly variable genes. (c) Cell clustering and type annotation. (d) Cell type composition across samples. (e) Comparative proportions between the CRC and the healthy control groups. (f) Localization of

CXCL12 and biomarkers in CRC. (g) CXCL12 levels across cell types in CRC versus healthy controls. (h) Differentiation pseudotime trajectory in the key population. (i) Intercellular communication networks in CRC and control groups.

CXCL12 expression controlled by MEIS2 and TCF4

Bioinformatics findings revealed substantial downregulation of CXCL12 and the three biomarkers in CRC tissues across training and validation cohorts. Concordantly, HT-29 colorectal cancer cells exhibited markedly lower mRNA levels of CXCL12 and biomarkers compared to normal FHC colonic cells ($p < 0.05$) **(Figure 5a).** Protein abundance of CXCL12 and associated biomarkers was similarly reduced in HT-29 cells ($p < 0.05$) **(Figure 5b).** These observations aligned fully with prior analytical results.

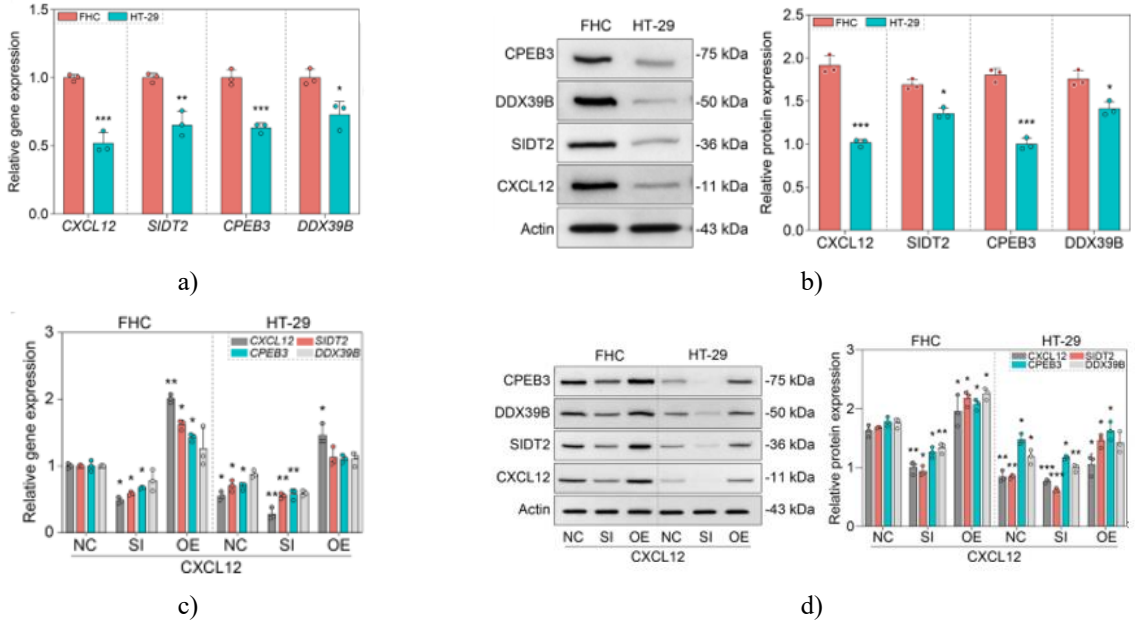

Figure 5. Assessment of CXCL12 and biomarker expression. (a) mRNA levels of CXCL12 and associated biomarkers (SIDT2, CPEB3, DDX39B) across groups (FHC and HT-29 cell lines). (b) Protein abundance of CXCL12 and biomarkers across groups (FHC and HT-29 cell lines). (c) mRNA expression of CXCL12 and CRC biomarkers in modified models (FHC-NC, FHC-siCXCL12, FHC-oeCXCL12, HT-29-NC, HT-29-siCXCL12, and HT-29-oeCXCL12). (d) Protein levels of CXCL12 and CRC biomarkers in the same modified models (FHC-NC, FHC-siCXCL12, FHC-oeCXCL12, HT-29-NC, HT-29-siCXCL12, and HT-29-oeCXCL12). $p < 0.05$, $p < 0.01$, $p < 0.001$, $p < 0.0001$.

qRT-PCR and Western blot analyses in CXCL12-knockdown and overexpression models of FHC and HT-29 cells demonstrated reduced CXCL12 levels in siCXCL12 conditions and elevated levels in oeCXCL12 conditions relative to respective negative controls (FHC-NC/HT-29-NC). In general, CXCL12, CPEB3, DDX39B, and SIDT2 exhibited higher abundance in FHC-derived cells, following this hierarchical pattern: highest in FHC-oeCXCL12, then FHC-NC, FHC-siCXCL12, HT-29-oeCXCL12, HT-29-NC, and lowest in HT-29-siCXCL12 **(Figures 5c–d).**

Identification of MEIS2 and TCF4 as regulatory transcription factors via single-cell TF profiling **(Figure 6a)** showed markedly elevated CXCL12 expression in oe-MEIS2 and oe-TCF4 HT-29 cells by qRT-PCR and Western blot **(Figures 6b–c).** Dual-luciferase allele-specific reporter assays further indicated dysregulated CXCL12 transcription linked to these upstream TFs **(Figure 6d).**

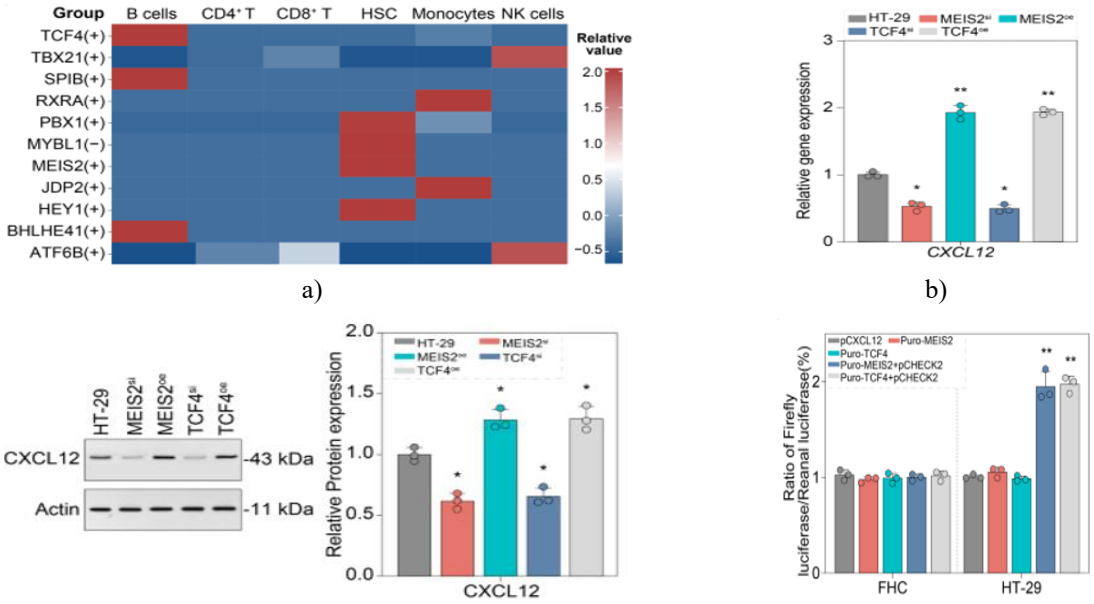

Figure 6. Investigation of CXCL12 transcriptional control. (a) Single-cell transcription factor profiling. (b) mRNA levels of CXCL12 across groups (HT-29-NC, siMEIS2, oeMEIS2, siTCF4, and oeTCF4). (c) Protein levels of CXCL12 across the same groups (HT-29-NC, siMEIS2, oeMEIS2, siTCF4, and oeTCF4). (d) Outcomes from dual-luciferase allele-specific expression reporter assays. $p < 0.05$, $p < 0.01$, $p < 0.001$, $p < 0.0001$.

CXCL12 knockdown enhances proliferation, migration, and invasion in CRC Cells

CCK-8 assays revealed significantly higher OD450 values in siCXCL12 cells compared to matched controls ($p < 0.05$) **(Figure 7a).**

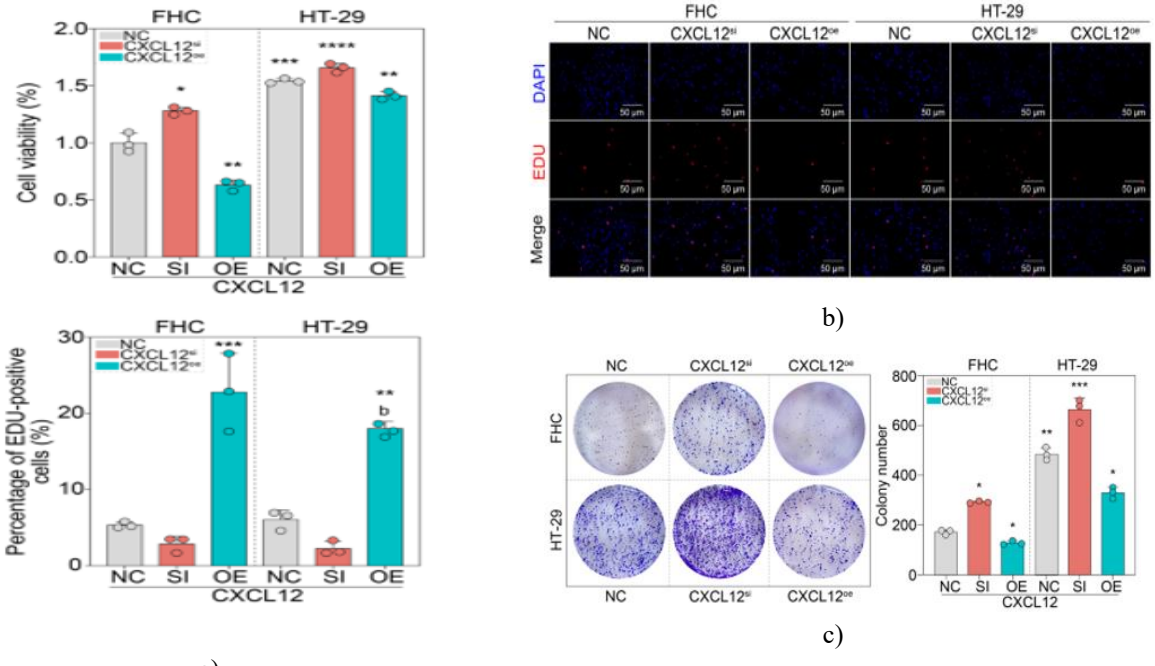

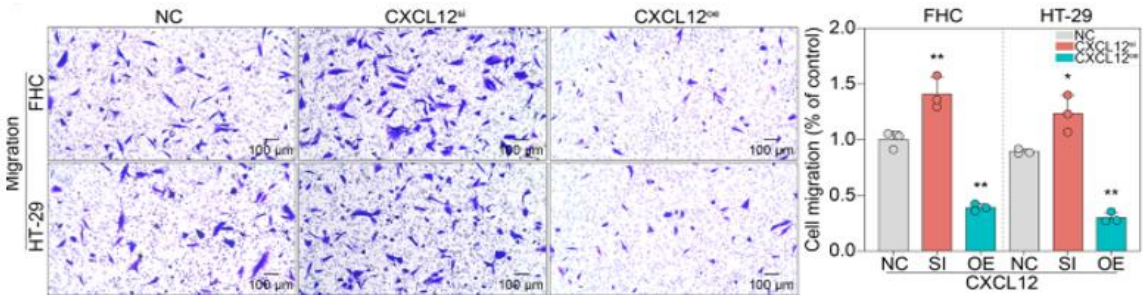

d)

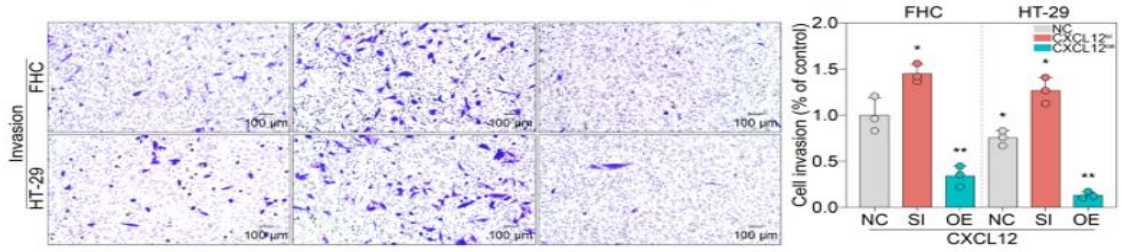

e)

Figure 7. Impact of CXCL12 modulation on CRC cell functional capacities. (a) Viability across cell models (FHC-NC, FHC-siCXCL12, FHC-oeCXCL12, HT-29-NC, HT-29-siCXCL12, and HT-29-oeCXCL12). (b) Proliferation rates per group. (c) Colony counts per group. (d) Migration ability per group. (e) Invasion ability per group. Letters a–d denote intergroup differences. NC: negative control; SI: knockdown (CXCL12 interference); OE: overexpression (CXCL12 vector). $p < 0.05$, $p < 0.01$, $p < 0.001$, $p < 0.0001$.

EdU incorporation displayed elevated red/blue fluorescence ratios in siCXCL12 conditions and reduced ratios in oeCXCL12 conditions, with stronger signals in knockdown cells versus controls ($p < 0.05$) **(Figure 7b).** Colony formation assays indicated reduced colony numbers in controls relative to siCXCL12 cells ($p < 0.05$) **(Figure 7c).** Together, these data confirm that CXCL12 suppression augments proliferative potential in CRC cells.

Transwell assays demonstrated substantially greater migrated and invaded cell counts in siCXCL12 groups compared to others ($p < 0.05$) **(Figures 7d–e),** indicating that CXCL12 downregulation facilitates enhanced migration and invasion in CRC cells.

In vivo CXCL12 suppression promotes CRC cell proliferation

Tumor-bearing Model mice developed rapidly progressing and larger neoplasms than controls **(Figure 8a)**. Relative to healthy controls, Model mice exhibited glandular disruption, pronounced cellular pleomorphism, enlarged hyperchromatic nuclei, nuclear-cytoplasmic ratio imbalance, and extensive tissue invasion. Lymph node sections from HT-29-NC injected mice versus HT-29-siCXCL12 injected mice revealed increased tumor cell dissemination in the latter **(Figure 8b).** Ki-67 staining was more intense in experimental tumors than controls, corroborating elevated proliferative activity upon CXCL12 inhibition in vivo **(Figure 8c).**

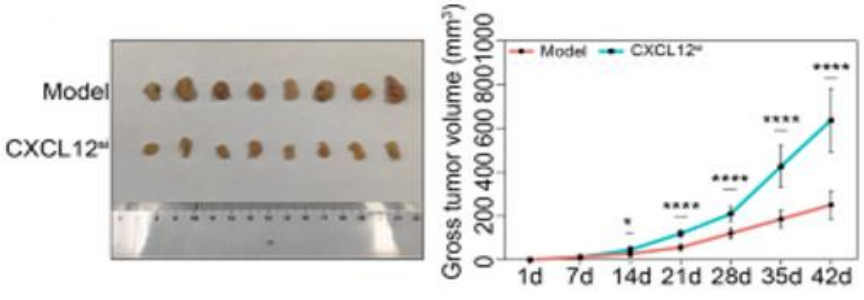

a)

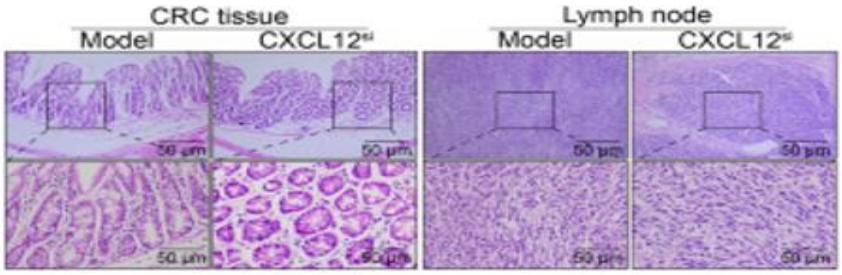
CRC tissue
Lymph node
Model
CXCL12si
50 μm

b)

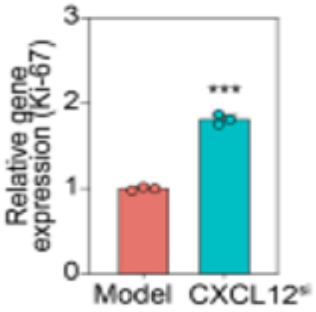
Relative gene expression (Ki-67)
***
Model
CXCL12si

c)

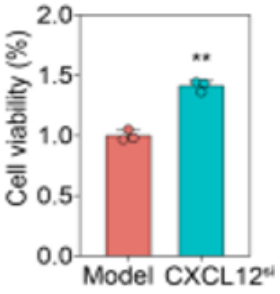
Cell viability (%)
**
Model
CXCL12si

d)

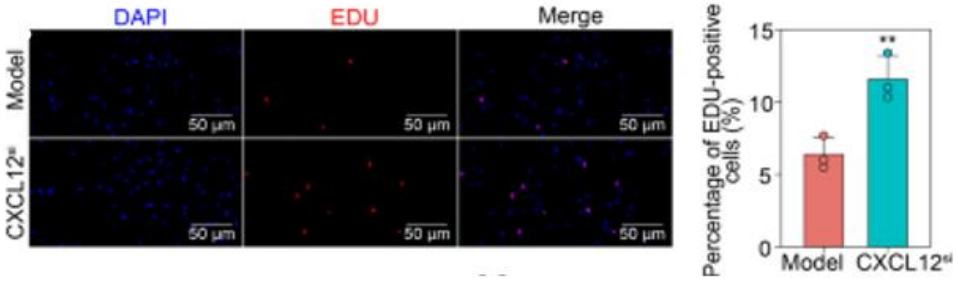
DAPI
EDU
Merge
Model
CXCL12si
50 μm
Percentage of EDU-positive cells (%)
Model
CXCL12si

e)

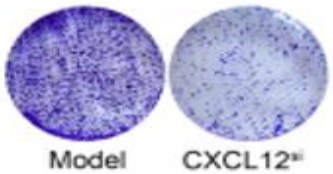
Model
CXCL12si

f)

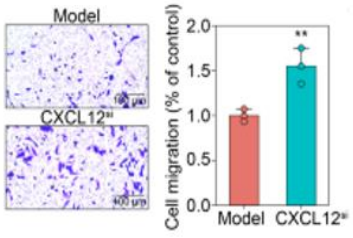
Model
CXCL12si
Cell migration (% of control)
Model
CXCL12si

g)

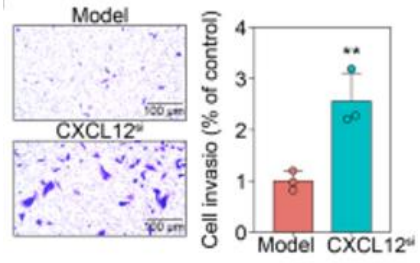
Model
CXCL12si
Cell invasio (% of control)
Model
CXCL12si

h)

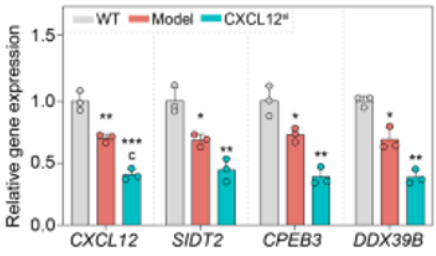
WT
Model
CXCL12si
Relative gene expression
CXCL12
SIDT2
CPEB3
DDX39B

i)

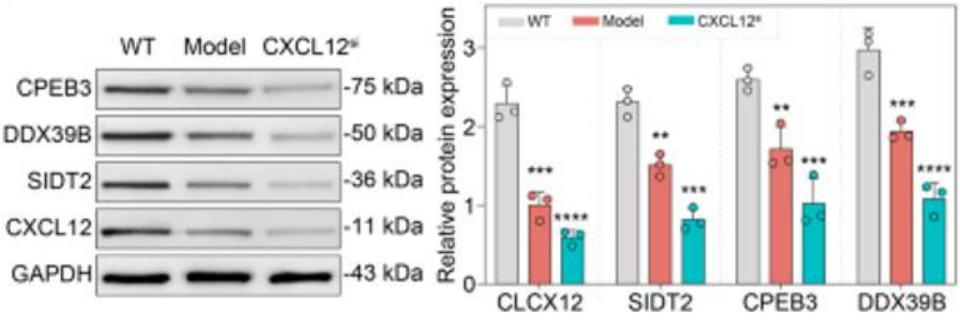

j)

Figure 8. The impact of CXCL12 suppression on cellular proliferation in vivo. (a) Tumor volume and progression tracked across 6 weeks. * denotes the 6-week feeding period. (b) H&E staining of colorectal tissue and lymph nodes from the Model and siCXCL12-Model mouse cohorts. (c) Ki-67 relative expression levels in the Model and siCXCL12-Model mouse cohorts. (d) Tumor cell viability in the Model and siCXCL12-Model mouse cohorts. (e) EdU incorporation assay outcomes. (f) Colony formation assay results. (g) Migratory ability of tumor cells from the Model and siCXCL12-Model mouse cohorts. (h) Invasive potential in the Model and siCXCL12-Model mouse cohorts. (i) Relative mRNA expression of CXCL12 and associated biomarkers across WT, Model, and siCXCL12-Model mouse cohorts. (j) Relative protein levels of CXCL12 and biomarkers in the WT, Model, and siCXCL12-Model mouse cohorts. Letters a–c indicate inter-group differences. * indicates $p < 0.05$, ** indicates $p < 0.01$, *** indicates $p < 0.001$, **** indicates $p < 0.0001$.

Consistent with in vitro findings, the CCK-8 assay revealed higher proliferative activity in the control group **(Figure 8d).** The ratio of red to blue fluorescence in the EdU assay was reduced in the treatment group compared to the control **(Figure 8e).** Likewise, colony numbers were fewer in the treatment group relative to the control **(Figure 8f).** Taken together, these data demonstrate that downregulation of CXCL12 expression leads to enhanced cellular proliferation. Transwell assays indicated significantly higher numbers of migrated and invaded cells in the treatment group compared to controls ($p < 0.05$) **(Figures 8g–h),** implying that CXCL12 knockdown facilitates migration and invasion of colorectal cancer cells. Gene and protein expression profiles of CXCL12 and related biomarkers in the WT, Model, and siCXCL12-Model cohorts aligned closely with the in vitro observations **(Figures 8i–j).**

CXCL12 overexpression improves the effectiveness of anti-PD-L1 therapy through decreased MDSC recruitment

Assessment of proliferative capacity using Con, CXCL12si, CXCL12oe, Con + anti-PD-L1, and CXCL12oe + anti-PD-L1 groups revealed a clear pattern: CXCL12si exhibited the greatest cell viability, followed sequentially by Con, CXCL12oe, Con + anti-PD-L1, with CXCL12oe + anti-PD-L1 displaying the lowest viability **(Figures 9a–b).** Migration and invasion rates followed an identical sequence, with CXCL12si highest and CXCL12oe + anti-PD-L1 lowest **(Figures 9c–d).** These observations indicate that elevated CXCL12 expression renders HT-29 cells more responsive to anti-PD-L1 therapy, as evidenced by the markedly reduced proliferation, migration, and invasion in the CXCL12oe + anti-PD-L1 combination, reflecting improved treatment outcome rather than therapeutic resistance.

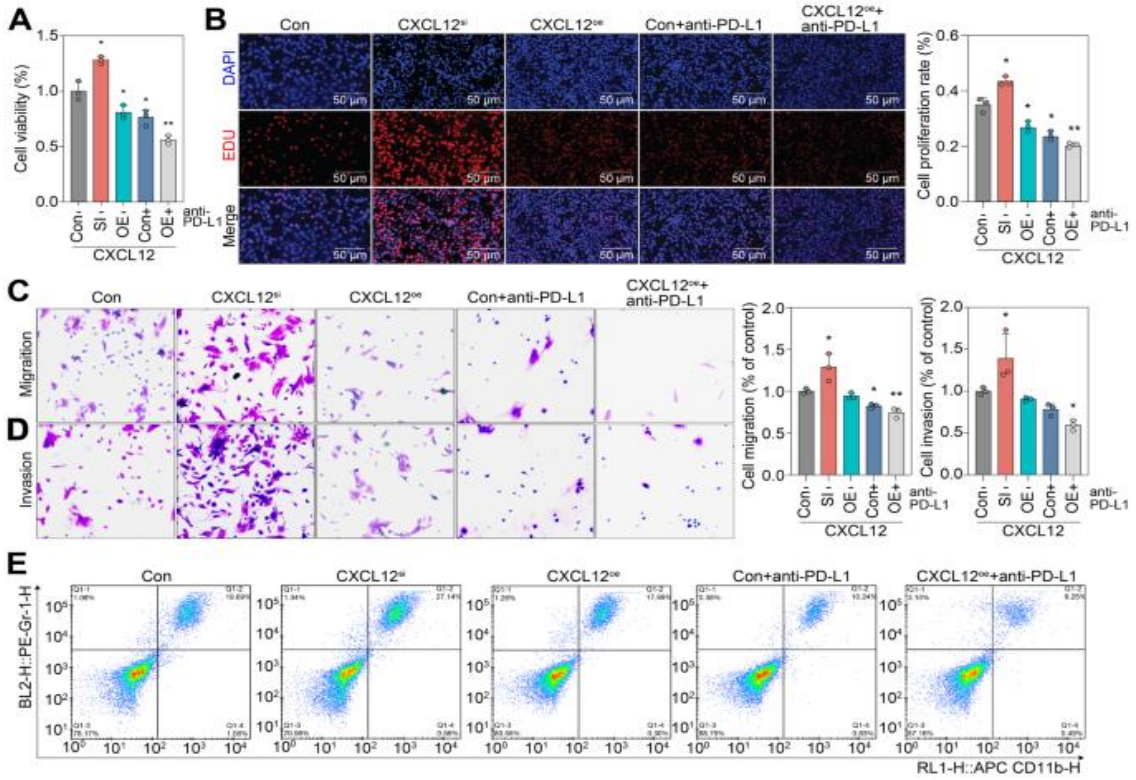

Figure 9. Elevated CXCL12 improves anti-PD-L1 response through diminished MDSC recruitment. (a) Viability profiles across treatment arms (con, CXCL12si, CXCL12oe, con + anti-PD-L1, CXCL12oe + anti-PD-L1). (b) Growth rates in various arms. (c) Migration outcomes across arms. (d) Invasion outcomes across arms. (e) Flow cytometric assessment of MDSC proportion and count shifts. Letters a–d signify group distinctions. $p < 0.05$, $p < 0.01$, $p < 0.001$, $p < 0.0001$.

Co-incubation of peripheral blood mononuclear cells with the five treatment variants, followed by flow cytometric quantification of critical populations, disclosed this MDSC abundance sequence: maximal in CXCL12si, then Con, CXCL12oe, Con + anti-PD-L1, and minimal in CXCL12oe + anti-PD-L1 **(Figure 9e),** paralleling the observed proliferation patterns.

The present investigation demonstrates that low CXCL12 levels, as opposed to high levels, impair the effectiveness of anti-PD-L1 therapy in colorectal cancer (CRC), employing single-cell RNA sequencing approaches. We begin by addressing major insights from our initial evaluation of CXCL12 abundance across 33 cancer entities to frame the later CRC-focused results. The broad screening revealed variable dysregulation of CXCL12. Such variability arises because CXCL12 is primarily produced by stromal components to orchestrate cell movement, vessel formation, and immune cell influx. In cancers like DLBC and GBM, stromal activation drives elevated CXCL12 to support tumor advancement, whereas in CRC and BRCA, diminished stromal activity or elevated antagonist presence reduces its abundance. Additionally, tumor-intrinsic factors contribute significantly. Individual malignancies possess unique genomic alterations and epigenetic changes governing CXCL12 transcription. For instance, in colon adenocarcinoma (COAD), alterations in APC or KRAS disrupt Wnt/β-catenin or MAPK cascades, previously linked to suppressed CXCL12 production. Conversely, EGFR mutations in GBM can stimulate PI3K/Akt signaling, enhancing CXCL12 output. Furthermore, tumor stage at diagnosis and tissue sampling procedures may influence observed levels. Here, comparisons involved neoplastic and peritumoral specimens from diverse sources, where variability in specimen consistency across malignancies likely amplified the discordant CXCL12 patterns.

Colorectal carcinogenesis follows a recognized sequence of genomic and epigenetic alterations [4]. Recent reports highlight pivotal contributions of RNA-binding proteins (RBPs) to CRC advancement, suggesting RBP-associated genes as potential diagnostic indicators and

modulators of tumor cell growth and motility [4, 6]. Our work identified 15 differentially expressed genes linked to CXCL12 that overlapped with RBP targets. Three (CPEB3, RBM20, and RBM6) correlated with improved CRC prognosis, while nine (DDX39B, IGHMBP2, MYEF2, NANOS1, RBPMS2, SAMHD1, SIDT2, TDRD9, and ZGPAT) correlated with poorer prognosis. This represents the initial evidence directly connecting these genes to CRC clinical trajectories, and the association of CXCL12-modulated RBPs with disease outcomes constitutes an original contribution.

Deeper examination of seven selected targets (CPEB3, DDX39B, NANOS1, RBM20, RBPMS2, SIDT2, and ZGPAT) confirmed involvement of CPEB3, DDX39B, and RBM20 in CRC pathogenesis, aligning with earlier reports [27-29]. The PI3K-Akt cascade primarily governs cellular expansion and oncogenic transformation in CRC. Certain investigations document aberrant pathway hyperactivity promoting accelerated tumor cell division [30]. Moreover, genetic changes or dysregulated components within PI3K/AKT strongly predict patient survival. Notably, PIK3CA alterations occur in approximately 17% of cases, often linked to reduced lifespan [31].

Comparable prognostic implications apply to elements of the Ras cascade, which predominantly drives CRC expansion and dissemination [32, 33]. RAS mutations dominate CRC genomics, with KRAS comprising 44.7% and NRAS 7.5% of relevant changes [33, 34]. Our data offer fresh support for CXCL12's substantial influence on both PI3K-Akt and Ras networks critical to CRC evolution.

CXCL12 acts as a chemoattractant that promotes cell translocation via CXCR4 engagement [35, 36]. This binding triggers G-protein signaling, leading to subunit separation into GTP-Gα, GTP-Gβ, and GTP-Gγ forms. These then stimulate downstream Ras/ERK, PLC-β, and PI3K/AKT routes [14, 15, 35, 37]. Drawing on this foundation, we hypothesized that PI3K-Akt and Ras pathways represent central RBP-influenced axes in CRC. Surprisingly, the consistently elevated diagnostic performance (AUC > 0.7) of CPEB3, DDX39B, and SIDT2 across training and external cohorts prompted their selection as CRC markers and formation of a CXCL12-based survival prediction framework.

The three chosen biomarkers operate within translational control governed by CPEB family members. Functions of CPEBs are extensively documented, encompassing modulation of cell cycle progression, senescence induction, and neuronal synaptic strengthening [38, 39]. Reduced CPEB3 abundance in colorectal tumor specimens strongly correlates with adverse patient outcomes [9], consistent with our observations. Prior work demonstrated that diminished CPEB3 accelerates CRC cell growth, motility, and invasiveness in both cultured and animal models, whereas forced expression suppresses these traits via disrupted JAK/STAT cascade hyperactivity [9]. Additional investigations indicate CPEB3 restrains epithelial-mesenchymal transition (EMT) by targeting IL-6R/STAT3 signaling, thereby interrupting interactions between neoplastic cells and tumor-associated macrophages [27].

Likewise, DDX39B emerges as a marker linked to unfavorable CRC survival [28, 40]. Growing data implicate DDX39B in driving CRC advancement through diverse routes, including facilitation of motility and EMT via the DDX39B/FUT3/TGFβR-I pathway [41], and direct promotion of cell division through binding to the CDK6/CCND1 assembly [42]. While SIDT2's involvement in CRC remains unexplored, marked downregulation has been noted across multiple malignancies, correlating with dismal prognosis and tied to enhanced proliferation, vessel formation, and tumor cell dissemination [43-45]. Remarkably, our cellular and animal manipulations of CXCL12 yielded highly comparable phenotypic outcomes.

Here, monocytes were designated as the principal CRC-associated population based on biomarker (CPEB3, DDX39B, and SIDT2) localization patterns. Monocytes constitute vital immune elements, contributing to systemic defense and inflammation [46]. Inflammation profoundly influences CRC initiation and progression, with monocytes capable of altering tumor expansion, invasion, and spread through secretion of cytokines and mediators [47]. Our analyses detected amplified intercellular signaling involving monocytes with CD8+ T cells, NK cells, and hematopoietic stem cells in CRC specimens. Prominently, MIF-(CD74+CXCR4) represented the dominant pair between hematopoietic stem cells and CD8+ T cells, while ANXA1–FPR1 prevailed between hematopoietic stem cells and monocytes. Prior reports propose that heightened MIF-(CD74+CXCR4) signaling impairs antitumor responses [48]. This same axis has been implicated in generating neutrophil extracellular traps linked to inflammatory periodontal damage [49]. The ANXA1–FPR1 interaction similarly supports tumor growth and invasiveness [50, 51]. Additional evidence links preoperative lymphocyte-

to-monocyte ratios to CRC survival, where lower ratios predict worse outcomes [47, 52].

Monocyte levels also align with broader inflammation metrics, including neutrophil-to-lymphocyte ratio and systemic immune-inflammation index (SII), both useful for CRC forecasting and outcome assessment [53]. Collectively, these insights suggest that signaling between CXCL12-responsive monocytes and surrounding immune subsets critically drives CRC cell proliferation and motility. For instance, PD-L1 acts as an immune checkpoint that fosters resistance via PD-1 binding [54]. Even so, anti-PD-L1 therapies can encounter resistance in some settings through TGF-β/Smad/EMT activation [54, 55].

As a chemokine, CXCL12 exerts major influence within the tumor milieu, particularly in CRC, by governing primary resistance to PD-L1 blockade via varied pathways; elucidating these is crucial for addressing immunotherapy hurdles and identifying reversal approaches [12, 56, 57]. The CXCL12–CXCR4 partnership stimulates CRC cell growth, invasiveness, and dissemination [13]. Higher CXCL12 correlates with later stages and poorer prognosis. This binding activates oncogenic cascades such as PI3K/AKT/mTOR, MEK/ERK, and Wnt/β-catenin, while reshaping immune dynamics in the microenvironment [16-18]. Our assessments of tumor cell growth and motility, including conditions with added CXCL12 or PD-L1 blockade, showed elevated activities when combining PD-L1 inhibition with CXCR4 antagonism, matching published data. Nonetheless, CXCL12 further shapes immune infiltration and polarization, thereby controlling PD-L1 behavior.

Evidence indicates CXCL12 enables immune escape through several routes. It promotes recruitment and stimulation of regulatory T cells alongside other suppressive lineages producing IL-10 and TGF-β to dampen effector T responses. Concurrently, CXCL12 elevates PD-L1 on tumor cells, establishing an immunosuppressive setting that hinders T cell killing [58, 59]. In our tumor-focused CRC system, CXCL12 depletion expanded MDSCs and diminished anti-PD-L1 responsiveness. By contrast, in malignancies dominated by cancer-associated fibroblast-derived CXCL12, the impact may reverse.

Notably, CXCL12's contribution to immunotherapy resistance extends beyond CRC, though its operative pathways differ by malignancy, revealing shared elements alongside tumor-type peculiarities. In pancreatic ductal adenocarcinoma (PDAC), marked by profound immunosuppression and limited immunotherapy success, CXCL12/CXCR4 activity chiefly fosters stromal fibrosis. CAF-produced CXCL12 attracts CXCR4-expressing suppressive leukocytes and impedes effector T cell penetration into tumor centers, thus conferring resistance to PD-1/PD-L1 inhibition [13, 14]. Distinct from CRC—where CXCL12 governs monocyte conversion to MDSCs—PDAC resistance relies predominantly on stromal-neoplastic interplay instead of direct immune lineage steering [60]. In non-small cell lung cancer (NSCLC), CXCL12 additionally fosters EGFR-TKI alongside anti-PD-L1 resistance by stimulating PI3K/AKT to boost PD-L1 while providing EGFR-bypassing survival cues [61]. Conversely, in breast carcinoma, CXCL12/CXCR4 drives PD-L1 inhibitor evasion via augmented EMT and cancer stemness, with little dependence on MDSC involvement—unlike the MDSC-focused process seen in CRC [62]. Such inter-tumor contrasts emphasize CXCL12 as a recurring mediator of immunotherapy failure, yet its effector cascades and cellular foci remain markedly tumor-dependent. This variability stems largely from organ-specific tumor microenvironment traits in CRC. CRC's TME displays a distinct immune profile, featuring elevated monocyte and MDSC fractions that offer an expanded reservoir for CXCL12-directed differentiation and immune suppression. These organ-unique features and comparative analyses carry substantial therapeutic relevance. For instance, CXCR4 blockers yielded modest benefits in PDAC owing to fibrotic obstacles [15], whereas our data imply greater potential in CRC through interruption of CXCL12-induced monocyte-to-MDSC shift; such agents might restore anti-PD-L1 sensitivity without necessitating stromal breakdown. Nonetheless, our evidence stresses incorporating CRC-particular elements in CXCL12-directed treatments, advocating biomarker-guided patient selection. Overall, within our neoplasm-centered framework, CXCL12 exerts a safeguarding role; its absence intensifies aggressiveness and M-MDSC proliferation, consequently impairing anti-PD-L1 performance. This contrasts with CAF-sourced CXCL12 dominance in PDAC; thus, source cell and organ milieu account for divergent outcomes. Our results indicate that CXCL12 shortfall, not surplus, fosters innate resistance to PD-L1 blockade via heightened MDSC influx and ensuing immune dampening.

In summary, this work uncovers a fresh pathway by which CXCL12 shortfall in colorectal tumor cells accelerates oncogenic advancement via dual-linked routes [1]: immediate amplification of neoplastic growth, motility, and invasiveness, and [2] secondary facilitation of MDSC buildup, generating a suppressive milieu that undermines anti-PD-L1 treatment success. This bipartite process rationalizes why CXCL12 augmentation, instead of blockade, emerges as an attractive approach to bolster PD-L1-targeted immunotherapy in CRC.

Conclusion

Multiple approaches to counteract CXCL12-related effects in CRC were explored herein, encompassing CXCR4 inhibitors, pathway blockers, immune-based treatments, and genetic interventions. CXCL12 reduction drives innate resistance to PD-L1 agents by intensifying tumor cell expansion, invasiveness, and motility, whereas CXCL12 replenishment improves anti-PD-L1 outcomes through altered immune trafficking and phenotype shifts, potentially via multifaceted (including cooperative) interplay with PD-L1 in CRC. Accordingly, tactics focused on reinstating CXCL12 abundance and associated cascades could prove valuable to augment PD-L1 blockade performance and elevate its utility as CRC immunotherapy.

Acknowledgments: None

Conflict of Interest: None

Financial Support: None

Ethics Statement: None

References

1. Huang X, Zhu X, Yu Y, Zhu W, Jin L, Zhang X, et al. Dissecting miRNA signature in colorectal cancer progression and metastasis. Cancer Lett. 2021;31:66–82. https://doi.org/10.1016/j.canlet.2020.12.025.
2. Kuipers EJ, Grady WM, Lieberman D, Seufferlein T, Sung JJ, Boelens PG, et al. Colorectal cancer. Nat Rev Dis Primers. 2015;1:15065. https://doi.org/10.1038/nrdp.2015.65.
3. Shin AE, Giancotti FG, Rustgi AK. Metastatic colorectal cancer: mechanisms and emerging therapeutics. Trends Pharmacol Sci. 2023;44(4):222–36. https://doi.org/10.1016/j.tips.2023.01.003.
4. Li K, Huang F, Li Y, Li D, Lin H, Ni R, et al. Stabilization of oncogenic transcripts by the IGF2BP3/ELAVL1 complex promotes tumorigenicity in colorectal cancer. Am J Cancer Res. 2020;10:2480–94.
5. Gerstberger S, Hafner M, Ascano M, Tuschl T. Evolutionary conservation and expression of human RNA-binding proteins and their role in human genetic disease. Adv Exp Med Biol. 2014;825:1–55. https://doi.org/10.1007/978-1-4939-1221-6_1.
6. Pereira B, Billaud M, Almeida R. RNA-binding proteins in cancer: old players and new actors. Trends Cancer. 2017;3:506–28. https://doi.org/10.1016/j.trecan.2017.05.003.
7. Jang HH, Lee HN, Kim SY, Hong S, Lee WS. Expression of RNA-binding motif protein 3 (RBM3) and cold-inducible RNA-binding protein (CIRP) is associated with improved clinical outcome in patients with colon cancer. Anticancer Res. 2017;37:1779–85. https://doi.org/10.21873/anticanres.11511.
8. Long Y, Marian TA, Wei Z. ZFR promotes cell proliferation and tumor development in colorectal and liver cancers. Biochem Biophys Res Commun. 2019;513:1027–34. https://doi.org/10.1016/j.bbrc.2019.04.103.
9. Fang Y, Zhong Q, Wang Y, Gu C, Liu S, Li A, et al. CPEB3 functions as a tumor suppressor in colorectal cancer via JAK/STAT signaling. Aging (albany, NY). 2020;12:21404–22. https://doi.org/10.18632/aging.103893.
10. Zeng Z, Yang H, Xiao S. ACTL6A expression promotes invasion, metastasis and epithelial mesenchymal transition of colon cancer. BMC Cancer. 2018;18:1020. https://doi.org/10.1186/s12885-018-4931-3.
11. Lin H, Zhang Y, Wang H, Xu D, Meng X, Shao Y, et al. Tissue inhibitor of metalloproteinases-3 transfer suppresses malignant behaviors of colorectal cancer cells. Cancer Gene Ther. 2012;19:845–51. https://doi.org/10.1038/cgt.2012.70.
12. Akishima-Fukasawa Y, Nakanishi Y, Ino Y, Moriya Y, Kanai Y, Hirohashi S. Prognostic significance of CXCL12 expression in patients with colorectal carcinoma. Am J Clin Pathol. 2009;132:202–10;

quiz 307. doi: https://doi.org/10.1309/AJCPK35VZJEWCUTL.
13. Goïta AA, Guenot D. Colorectal cancer: the contribution of CXCL12 and its receptors CXCR4 and CXCR7. cancers (Basel). 2022;14(7):1810. https://doi.org/10.3390/cancers14071810.
14. Biasci D, Smoragiewicz M, Connell CM, et al. CXCR4 inhibition in human pancreatic and colorectal cancers induces an integrated immune response. Proc Natl Acad Sci U S A. 2020;117(46):28960–70. https://doi.org/10.1073/pnas.2013644117.
15. Khare T, Bissonnette M, Khare S. CXCL12-CXCR4/CXCR7 axis in colorectal cancer: therapeutic target in preclinical and clinical studies. Int J Mol Sci. 2021;22(14):7371. https://doi.org/10.3390/ijms22147371.
16. Ma JC, Sun XW, Su H, Chen Q, Guo TK, Li Y, et al. Fibroblast-derived CXCL12/SDF-1α promotes CXCL6 secretion and co-operatively enhances metastatic potential through the PI3K/Akt/mTOR pathway in colon cancer. World J Gastroenterol. 2017;23:5167–78. https://doi.org/10.3748/wjg.v23.i28.5167.
17. Daniel SK, Seo YD, Pillarisetty VG. The CXCL12-CXCR4/CXCR7 axis as a mechanism of immune resistance in gastrointestinal malignancies. Semin Cancer Biol. 2020;65:176–88. https://doi.org/10.1016/j.semcancer.2019.12.007.
18. Yu W, et al. The connection between surgical margins in liver metastases from colorectal cancer and patient prognosis: a mini review. Curr Probl Surg. 63(2025):101700. https://doi.org/10.1016/j.cpsurg.2024.101700.
19. Yang F, Cai S, Ling L, Zhang H, Tao L, Wang Q. Identification of a five-gene prognostic model and its potential drug repurposing in colorectal cancer based on TCGA, GTEx and GEO databases. Front Genet. 2021;11:622659. https://doi.org/10.3389/fgene.2020.622659.
20. Yue T, Chen S, Zhu J, Guo S, Huang Z, Wang P, et al. The aging-related risk signature in colorectal cancer. Aging (albany, NY). 2021;13:7330–49. https://doi.org/10.18632/aging.202589.
21. Xie S, Cai Y, Chen D, Xiang Y, Cai W, Mao J, Ye J. Single-cell transcriptome analysis reveals heterogeneity and convergence of the tumor microenvironment in colorectal cancer. Front Immunol. 2023;13:1003419. https://doi.org/10.3389/fimmu.2022.1003419.
22. Harris BHL, Di Giovannantonio M, Zhang P, Harris DA. Lord SR, Allen NE, et al. New role of fat-free mass in cancer risk linked with genetic predisposition. Sci Rep. 2024;14:7270. https://doi.org/10.1038/s41598-024-54291-7.
23. Võsa U, Claringbould A, Westra HJ, Bonder MJ, Deelen P, Zeng B, et al. Large-scale cis- and trans-eQTL analyses identify thousands of genetic loci and polygenic scores that regulate blood gene expression. Nat Genet. 2021;53:1300–10. https://doi.org/10.1038/s41588-021-00913-z.
24. Peng F, Muhuitijiang B, Zhou J, Liang H, Zhang Y, Zhou R. An artificial neural network model to diagnose non-obstructive azoospermia based on RNA-binding protein-related genes. Aging (albany, NY). 2023;15:3120–40. https://doi.org/10.18632/aging.204674.
25. Love MI, Huber W, Anders S. Moderated estimation of Fold change and dispersion for RNA-seq data with DESeq2. Genome Biol. 2014;15:550. https://doi.org/10.1186/s13059-014-0550-8.
26. Hao Y, Hao S, Andersen-Nissen E, Mauck WM, Zheng S, Butler A, et al. Integrated analysis of multimodal single-cell data. Cell. 2021;184:3573–87.e29. https://doi.org/10.1016/j.cell.2021.04.048.
27. Zhong Q, Fang Y, Lai Q, Wang S, He C, Li A, et al. CPEB3 inhibits epithelial-mesenchymal transition by disrupting the crosstalk between colorectal cancer cells and tumor-associated macrophages via IL-6R/STAT3 signaling. J Exp Clin Cancer Res. 2020;39:132. https://doi.org/10.1186/s13046-020-01637-4.
28. He Q, Li Z, Lei X, Zou Q, Yu H, Ding Y, et al. The underlying molecular mechanisms and prognostic factors of RNA binding protein in colorectal cancer: a study based on multiple online databases. Cancer Cell Int. 2021;21:325. https://doi.org/10.1186/s12935-021-02031-6.
29. Schmit SL, Tsai YY, Bonner JD, Sanz-Pamplona R, Joshi AD, Ugai T, et al. Germline genetic regulation of the colorectal tumor immune microenvironment. BMC Genomics. 2024;25:409. https://doi.org/10.1186/s12864-024-10295-1.
30. Wang M, Zhang H, Lu Z, Su W, Tan Y, Wang J, et al. PSAT1 mediated EMT of colorectal cancer cells by regulating Pl3K/AKT signaling pathway. J

Cancer. 2024;15:3183–98. https://doi.org/10.7150/jca.93789.
31. Christensen TD, Palshof JA, Larsen FO, Poulsen TS, Høgdall E, Pfeiffer P, et al. Associations between primary tumor RAS, BRAF and PIK3CA mutation status and metastatic site in patients with chemo-resistant metastatic colorectal cancer. Acta Oncol. 2018;57:1057–62. https://doi.org/10.1080/0284186X.2018.1433322.
32. Jiao HL, Weng BS, Yan SS, Lin ZM, Wang SY, Chen XP, et al. Upregulation of OSBPL3 by HIF1A promotes colorectal cancer progression through activation of RAS signaling pathway. Cell Death Dis. 2020;11:571. https://doi.org/10.1038/s41419-020-02793-3.
33. Bousquet MS, Ma JJ, Ratnayake R, Havre PA, Yao J, Dang NH, et al. Multidimensional screening platform for simultaneously targeting oncogenic KRAS and hypoxia-inducible factors pathways in colorectal cancer. ACS Chem Biol. 2016;11:1322–31. https://doi.org/10.1021/acschembio.5b00860.
34. Serebriiskii IG, Connelly C, Frampton G, Newberg J, Cooke M, Miller V, et al. Comprehensive characterization of RAS mutations in colon and rectal cancers in old and young patients. Nat Commun. 2019, Aug, 19;10(1):3722. https://doi.org/10.1038/s41467-019-11530-0.
35. Ottaiano A, Scala S, Normanno N, Botti G, Tatangelo F, Di Mauro A, et al. Prognostic and predictive role of CXC chemokine receptor 4 in metastatic colorectal cancer patients. Appl Immunohistochem Mol Morphol. 2020;28:755–60. https://doi.org/10.1097/PAI.0000000000000828.
36. Zheng F, Zhang Z, Flamini V, Jiang WG, Cui Y. The axis of CXCR4/SDF-1 plays a role in colon cancer cell adhesion through regulation of the AKT and IGF1R signalling pathways. Anticancer Res. 2017;37:4361–69. https://doi.org/10.21873/anticanres.11830.
37. De Mattia E, Bignucolo A, Toffoli G, Cecchin E. Genetic markers of the host to predict the efficacy of colorectal cancer targeted therapy. Curr Med Chem. 2020;27:4249–73. https://doi.org/10.2174/0929867326666190712151417.
38. Phesse TJ, Buchert M, Stuart E, Flanagan DJ, Faux M, Afshar-Sterle S, et al. Partial inhibition of gp130-jak-Stat3 signaling prevents wnt-β-catenin-mediated intestinal tumor growth and regeneration. Sci Signal. 2014;7:ra92. https://doi.org/10.1126/scisignal.2005411.
39. Groppo R, Richter JD. CPEB control of NF-kappaB nuclear localization and interleukin-6 production mediates cellular senescence. Mol Cell Biol. 2011;31:2707–14. https://doi.org/10.1128/MCB.05133-11.
40. Zhao G, Yuan H, Li Q, Zhang J, Guo Y, Feng T, et al. DDX39B drives colorectal cancer progression by promoting the stability and nuclear translocation of PKM2. Signal Transduct Target Ther. 2022;7:275. https://doi.org/10.1038/s41392-022-01096-7.
41. He C, Li A, Lai Q, Ding J, Yan Q, Liu S, et al. The DDX39B/FUT3/TGFβR-I axis promotes tumor metastasis and EMT in colorectal cancer. Cell Death Dis. 2021;12:74. https://doi.org/10.1038/s41419-020-03360-6.
42. Zhang H, He C, Guo X, Fang Y, Lai Q, Wang X, et al. DDX39B contributes to the proliferation of colorectal cancer through direct binding to CDK6/CCND1. Cell Death Discov. 2022;8:30. https://doi.org/10.1038/s41420-022-00827-7.
43. Yi D, Zhang D, He J. Long non-coding RNA LIFR-AS1 suppressed the proliferation, angiogenesis, migration and invasion of papillary thyroid cancer cells via the miR-31-5p/SIDT2 axis. Cell Cycle. 2021;20:2619–37. https://doi.org/10.1080/15384101.2021.1995129.
44. Nguyen TA, Bieging-Rolett KT, Putoczki TL, Wicks IP, Attardi LD, Pang KC. SIDT2 RNA transporter promotes lung and gastrointestinal tumor development. iScience. 2019;20:14–24. https://doi.org/10.1016/j.isci.2019.09.009.
45. Wang LJ, Chiou JT, Lee YC, Chang LS. Docetaxel-triggered SIDT2/NOX4/JNK/HuR signaling axis is associated with TNF-α-mediated apoptosis of cancer cells. Biochem Pharmacol. 2022;195:114865. https://doi.org/10.1016/j.bcp.2021.114865.
46. Deng D, Luo X, Zhang S, Xu Z. Immune cell infiltration-associated signature in colon cancer and its prognostic implications. Aging (albany, NY). 2021;13:19696–709. https://doi.org/10.18632/aging.203380.
47. Shimizu T, Ishizuka M, Shiraki T, Sakuraoka Y, Mori S, Abe A, et al. The clinical influence of the preoperative lymphocyte-to-monocyte ratio on the postoperative outcome of patients with early-stage gastrointestinal cancer. Ann Gastroenterol Surg. 2020;4:580–90. https://doi.org/10.1002/ags3.12369.

48. Wang Q, Liu W, Zhou H, Lai W, Hu C, Dai Y, et al. Tozasertib activates anti-tumor immunity through decreasing regulatory T cells in melanoma. Neoplasia. 2024;48:100966. https://doi.org/10.1016/j.neo.2024.100966.
49. Qiu W, Guo R, Yu H, Chen X, Chen Z, Ding D, et al. Single-cell atlas of human gingiva unveils a NETs-related neutrophil subpopulation regulating periodontal immunity. J Adv Res. 2024;72:287–301. https://doi.org/10.1016/j.jare.2024.07.028.
50. Motevasseli M, Darvishi M, Khoshnevisan A, Zeinalizadeh M, Saffar H, Bayat S, et al. Distinct tumor-TAM interactions in IDH-stratified glioma microenvironments unveiled by single-cell and spatial transcriptomics. Acta Neuropathol Commun. 2024;12:133. https://doi.org/10.1186/s40478-024-01837-5.
51. Vecchi L, Alves Pereira Zóia M, Goss Santos T, de Oliveira Beserra A, Colaço Ramos CM, França Matias Colombo B, et al. Inhibition of the AnxA1/FPR1 autocrine axis reduces MDA-MB-231 breast cancer cell growth and aggressiveness in vitro and in vivo. Biochim Biophys Acta Mol Cell Res. 2018;1865:1368–82. https://doi.org/10.1016/j.bbamcr.2018.06.010.
52. Koržinek M, Ćelap I, Fabijanec M, Žanić T, Ljubičić N, Baršić N, et al. Complete blood count parameters and inflammation-related biomarkers in patients with colorectal carcinoma. Acta Pharm. 2025;74:739–49. https://doi.org/10.2478/acph-2024-0036.
53. Kozak MM, von Eyben R, Pai JS, Anderson EM, Welton ML, Shelton AA, et al. The prognostic significance of pretreatment hematologic parameters in patients undergoing resection for colorectal cancer. Am J Clin Oncol. 2017;40:405–12. https://doi.org/10.1097/COC.0000000000000183.
54. Yuan Y, Adam A, Zhao C, Chen H. Recent advancements in the mechanisms underlying resistance to PD-1/PD-L1 blockade immunotherapy. Cancers (basel). 2021;13:663. https://doi.org/10.3390/cancers13040663.
55. Zhang Y, Zeng Y, Liu T, Du W, Zhu J, Liu Z, et al. The canonical TGF-β/Smad signalling pathway is involved in PD-L1-induced primary resistance to EGFR-TKIs in EGFR-mutant non-small-cell lung cancer. Respir Res. 2019;20:164. https://doi.org/10.1186/s12931-019-1137-4.
56. D'Alterio C, Giardino A, Scognamiglio G, Butturini G, Portella L, Guardascione G, et al. CXCR4-CXCL12-CXCR7 and PD-1/PD-L1 in pancreatic cancer: CXCL12 predicts survival of radically resected patients. Cells. 2022;11:3340. https://doi.org/10.3390/cells11213340.
57. Zeng Y, Li B, Liang Y, Reeves PM, Qu X, Ran C, et al. Dual blockade of CXCL12-CXCR4 and PD-1-PD-L1 pathways prolongs survival of ovarian tumor-bearing mice by prevention of immunosuppression in the tumor microenvironment. Faseb J. 2019;33:6596–608. https://doi.org/10.1096/fj.201802067RR.
58. Chang CY, Chang SC, Wei YF, Tseng YT, Chou CH, Chen YY, et al. Exploring the evolution of T cell function and diversity across different stages of non-small cell lung cancer. Am J Cancer Res. 2024;14:1243–57. https://doi.org/10.62347/ARYH6451.
59. Raufi AG, Pellicciotta I, Palermo CF, Sastra SA, Chen A, Alouani E, et al. Cytotoxic chemotherapy potentiates the immune response and efficacy of combination CXCR4/PD-1 inhibition in models of pancreatic ductal adenocarcinoma. bioRxiv. 2023. https://doi.org/10.1101/2023.12.24.573257.
60. Li Y, Zheng Y, Xu S, et al. The nanobody targeting PD-L1 and CXCR4 counteracts pancreatic stellate cell-mediated tumour progression by disrupting tumour microenvironment. Int Immunopharmacol. 2024;132:111944. https://doi.org/10.1016/j.intimp.2024.111944.
61. Xu Y, Ding L, Li H, et al. Serum cytokine analysis in a cohort of advanced non-small cell lung cancer treated with PD-1 inhibitors reveals predictive markers of CXCL12. Front Immunol. 2023;14:1194123. https://doi.org/10.3389/fimmu.2023.1194123. Published 2023 Jun 9.
62. Kravtsova-Ivantsiv Y, Goldhirsh G, Ciechanover A. CXCL12 restricts tumor growth by suppressing the ras, ERK1/2, c-myc, and the immune checkpoint PD-L1 pathways. Proc Natl Acad Sci U S A. 2024;121(52):e2416909121. https://doi.org/10.1073/pnas.2416909121.